Processing of Poly(2,6-dimethyl-1,4-phenylene ether) with Epoxy Resin. 1. Reaction-Induced Phase Separation

Yoshiyuki Ishii† and Anthony J. Ryan*

Department of Chemistry, The University of Sheffield, Brookhill, Sheffield, S3 7HF, UK

Received May 28, 1999; Revised Manuscript Received October 11, 1999

ABSTRACT: Poly(2,6-dimethyl-1,4-phenylene ether) (PPE) is difficult to process without the use of solvents. PPE was dissolved in epoxy resin, and reaction-induced phase separation in the blend was studied using a time-resolved, small-angle light-scattering camera equipped with a DSC stage. Laser light scattering measurements characterize the reaction-induced phase separation process. A four-stage model is discussed: (a) reaction prior to phase separation, (b) early stage of spinodal decomposition, (c) late stage of spinodal decomposition, and (d) refractive index changes and apparent phase dissolution. Cahn−Hilliard linear theory, yielding initial correlation lengths and effective interdiffusion coefficients, accounts for the early stage of phase separation by spinodal decomposition. In the late stage, the scattering peak position, q_m, starts to decrease with time according to a power law; however, the maximum in the scattered intensity, I_m, does not satisfy a power law due to the large change in the epoxy refractive index during cross-linking. The disperse-phase morphology and mechanical properties of the cured blend are investigated by SEM, TEM, and DMTA.

Introduction

Polymers are increasingly being used in a wide variety of applications in microelectronics.[1] Many applications require material properties that only polymers can provide, such as circuit boards, integrated circuit (IC) packages, cable insulation, encapsulants, adhesives, resist materials for the lithographic fabrication of IC, and materials for optical recording. Many studies of electronic applications of polymers have been made,[2] and rapid development is apparent in areas where polymer science intersects with semiconductor device fabrication, dielectric materials, information storage media, and organic conductors. One major emphasis has been the research of electronic properties in situations in which polymer acts as an insulating material. Increasing miniaturization is causing increasing circuit density, and stringent environmental regulations have been dominant.[3] As insulating materials, printed circuit boards have played a significant role in the development of a sophisticated information society. Poly(2,6-dimethyl-1,4-phenylene ether) (PPE) has a low dielectric constant of 2.45, a low dissipation factor of 0.0007, and high glass transition temperature (T_g) of 210 °C.[4] PPE is one of the candidates to satisfy the demand of the electronics industry; however, a high T_g is often obtained at the cost of difficult processing. One way to reduce the viscosity of thermoplastics during processing is by using solvents. This, however, incurs significant disadvantages during and after processing. First, it requires the disposal or discharge of organic solvent. Second, volatilization of the solvent from the material can result in the presence of voids and irregularities in the material. Furthermore, a considerable amount of time is required for the solvent removal stage. These problems could be surmounted by dissolving a thermoplastic in thermosetting monomers. Instead of solvent removal during processing, thermosets can be polymerized into a constituent of the final material. By choosing an appropriate thermoset for the purpose, reduction of the thermoplastics T_g may be prevented. This concept was defined as "reactive solvent" by Venderbosch.[5−7]

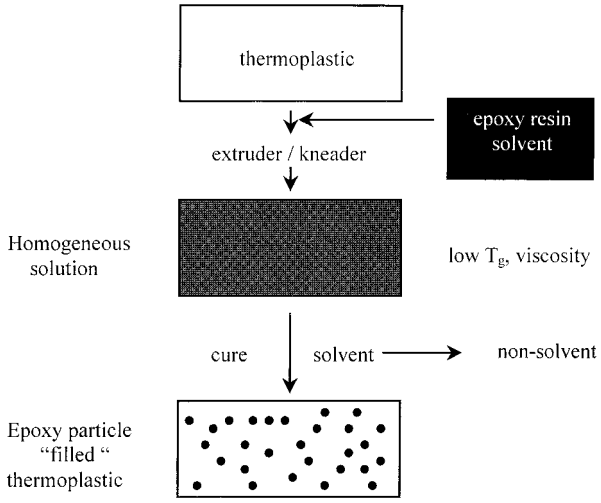

Figure 1. Schematic representation of the concept of processing of intractable polymers using reactive solvents.[5]

Venderbosch studied the PPE/epoxy resin system for composites[7] and observed that the diglycidyl ether of bisphenol A epoxy (DGEBA) is an excellent reactive solvent for PPE. The basic idea is to leave the solvent within the product after having made it harmless by polymerization; this is shown schematically in Figure 1. In PPE/DGEBA epoxy mixtures, an upper critical solution temperature (UCST) phase diagram was observed. During processing, the solvent gives a large reduction in the processing temperature or decreases the viscosity of the polymer. After shaping, the solvent is converted into a nonsolvent induced by polymerization. In the composition range from 20 to 50 wt % of PPE, phase separation is accompanied by phase inversion, yielding a final morphology of epoxy-rich spheres dispersed in a PPE-rich matrix. This phase separation

† Current address: Fabrication Technology Laboratory, Asahi Chemical Industry, Co., Ltd. Yakoh, Kawasaki, 210-0863 Japan.
* To whom all correspondence should be addressed.

10.1021/ma990837i CCC: $19.00
Published on Web 12/18/1999

is called "reaction-induced phase separation" or "chemically induced phase separation" compared to "thermally induced phase separation".[8] A dispersed phase results, locking the original solvent inside the thermoplastic matrix material that forms the continuous phase. Reaction-induced phase separation is the structure development mechanism in a wide range of materials such as polyurethanes,[9] IPNs,[10] rubber-modified epoxies,[11] and thermoplastic/thermoset alloys.[12] It is obvious that both physical events (reaction-induced phase separation, vitrification) and chemical events (cross-linking, gelation) are occurring during processing. For such a technology to progress up to an industrialized level, it is necessary to understand both physical and chemical events during processing.

In this paper, reaction-induced phase separation of PPE/epoxy blends is investigated using a specially constructed time-resolved light scattering camera equipped with a DSC. Laser light scattering measurements characterize the subsequent spinodal decomposition process. The development of molar mass in the epoxy resin is gradual. The step-growth mechanism means the molar mass evolves slowly with conversion, and the reaction mixture has a molar mass distribution that is continuous. Nonlinear step polymerizations also have continuous molecular distributions throughout the reaction; this is manifest in the chemical gel point not being a true phase transition and the reaction remaining homogeneous throughout. For this reason the thermodynamics of mixtures of a homopolymer with a step polymerization may be considered to be those of a pseudobinary[8] where one phase is the homopolymer and the other is the reactant mixture. The phase boundary is located by the molar mass of the epoxy and for an isothermal cure passes through the composition−temperature point at which the reaction takes place.[5] Cahn−Hilliard linear theory,[13] yielding initial correlation lengths and effective interdiffusion coefficients, accounts for the early stage of the spinodal decomposition, and the phase-inverted morphology of the cured blend is confirmed by SEM, TEM, and DMTA.

Experimental Section

Poly(2,6-dimethyl-1,4-phenylene ether) (PPE) was supplied by Asahi Chemical Industry Co., Ltd. The number-average molecular weight (M_n) is 29 000, with a molecular weight distribution, characterized by M_w/M_n, of 1.45. The digycidyl ether of bisphenol A type epoxy resin (DGEBA) used in this study was Araldite AER 260 (AER260) supplied by Asahi-Ciba Ltd. The epoxide equivalent of AER 260 was 190.6 determined by titration.[14] Diethyltoluenediamine (DETDA) was used as hardener. This aromatic diamine is an 80:20 mixture of the 2,4- and 2,6-isomers supplied by Lonza AG. PPE, epoxy resin, and DETDA were used without further purification.

Mixing of PPE and epoxy resin was performed in a Brabender plastograph kneader. Samples were mixed at 185 °C for 1 h, and then the chamber was opened. The mixture was raked out immediately and cooled to room temperature. Mixtures having less than 20% PPE were prepared in a beaker with mechanical stirring. The Brabender plastograph kneader was also used for ternary mixture of PPE/epoxy/DETDA systems. Initially, PPE and epoxy were mixed at 185 °C for 1 h. The mixture was cooled to 150 °C, and a stoichiometric mass of DETDA was added using a syringe. After mixing for 2 min, the mixture was quickly removed and stored in a freezer at −30 °C.

Demixing of PPE/epoxy mixtures was confirmed by optical microscopy. Samples with various epoxy contents were placed into a Linkam THMS 600 hot stage between glass slides. Upon controlled cooling of the cell using a Linkam TMS 91 controller, the onset of phase separation was observed by using an Olympus BH-2 optical microscope equipped with a single lens reflex camera. Parallel-plate rheometry was used to measure viscosity, the storage and loss components of the complex shear modulus, and loss factor with respect to time and temperature. Measurements were made using the dynamic, multifrequency, oscillatory-shear mode on a Rheometrics RMS 800 rheometer. Differential canning calorimetry (DSC) was used to determine the T_g of PPE/epoxy blends and for kinetic studies of network formation. A Dupont 2000 thermal analyzer equipped with a DSC 990 cell was operated under a nitrogen atmosphere using samples of ∼10 mg encapsulated in aluminum pans. For the epoxy reaction kinetics two experimental methods were adopted. In dynamic DSC, the pan was cooled to −100 °C on the DSC head and then heated at 10 °C/min. Measurements of heat flow and against time and temperature were made, with respect to a reference. For isothermal measurements, a cold sample pan was inserted into the DSC which was maintained at the polymerization temperature. Thermal equilibrium was established in less than 1 min. The rate of enthalpy evolution was followed with time. The isothermal heat flow curve was obtained to subtract the baseline signal, assuming that the difference in heat capacity before and after reaction is negligible.

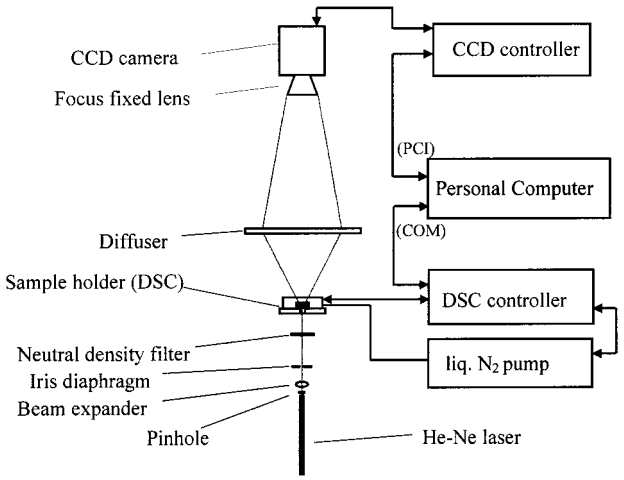

Figure 2. Schematic diagram of the general layout of the time-resolved light scattering with an optical DSC.

The morphology of the cured PPE/epoxy resin was observed by SEM (Philips, SEM 525) and TEM (Phillips EM400). For TEM, thin samples were prepared using an ultramicrotome (Ultracut, Reichert) to 70 nm. The specimens were transferred to the surface of a copper grid (400 mesh) and then stained using OsO_4 (2% solution). For SEM gold-coated fracture surfaces were used.

A time-resolved small-angle light scattering setup has been specially designed and constructed[15] as shown schematically in Figure 2. The scattering equipment comprises three parts, i.e., light source, sample holder, and detector. The light source is a 20 mW He−Ne laser, linearly polarized, with $\lambda = 632.8$ nm and a beam size at $1/e^2$ of 0.65 mm. The Linkam DSC (DSC optical cell) was adopted as a sample holder, and its operation and performance are described elsewhere.[16] Scattered light from the sample falls onto a diffuser, and a 512 × 512 pixel CCD camera (SITe 7130-0004, Princeton Instruments) is focused on the diffuser using a fixed focal length lens. Thus, the scattered light is imaged onto the CCD array. Data were recorded on a PC, and all the data processing was conducted on a Sun workstation using the CCP13 programs.[17] Real space images during reaction-induced phase separation, for comparison to the light scattering, were obtained from a JVC TK-C1381 CCD camera attached to the Olympus BH-2 microscope. The same model of DSC was used for the time-resolved light scattering and optical microscopy experiments.

The premixed samples were sliced and mounted into DSC pans, which had punched holes, and mica windows were made

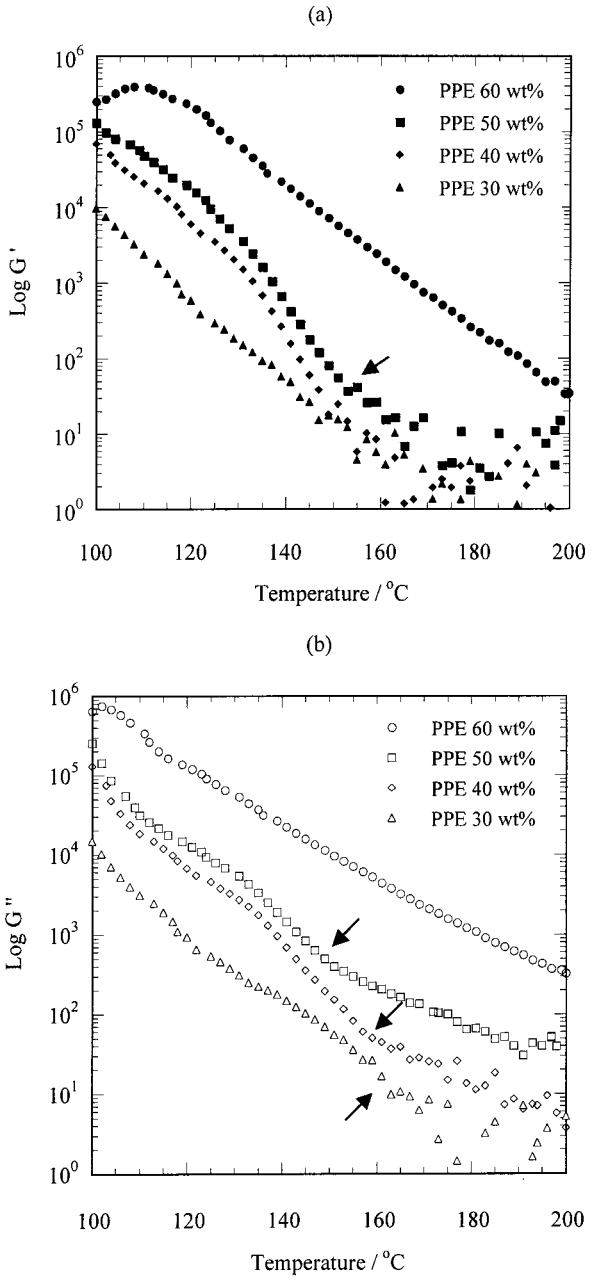

Figure 3. Rheology of PPE/epoxy mixture upon cooling from homogeneous solution: (a) storage modulus; (b) loss modulus. The arrows indicate the onset of phase separation.

to establish an optical path.[16] For isothermal measurements, the sample pan was inserted into the DSC stage at room temperature, and the temperature raised rapidly. As soon as the temperature reached the curing temperature, a series of scattering images were taken approximately every 5 s.

Results and Discussion

Phase Diagram of PPE/Epoxy System. The onset of phase separation of PPE/epoxy can be easily observed by optical microscopy as previously reported.[5] Rheological and calorimetric characteristics of the blend are also influenced by liquid−liquid phase separation. Figure 3 presents storage and loss moduli of different compositions of the PPE/epoxy mixture as a function of the temperature during cooling. These rheological data reflect the structure development on cooling. The onset of phase separation is distinguished as a discontinuity in G' and G'' due to the emergence of a PPE-rich phase

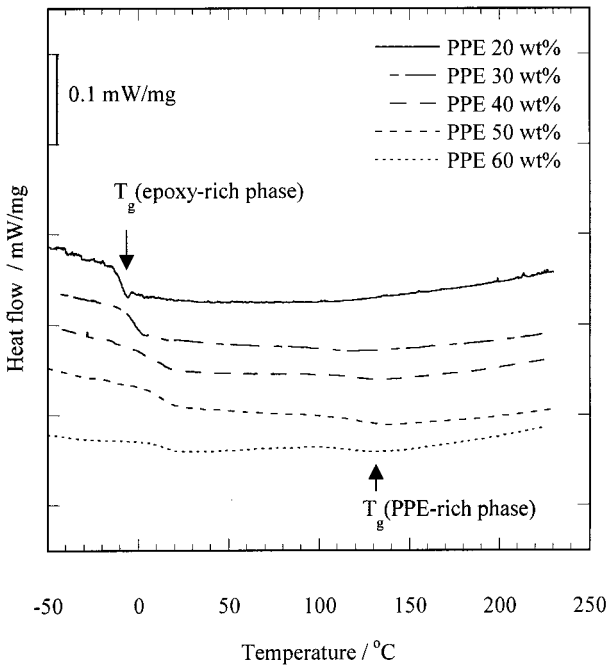

Figure 4. DSC curves of PPE/epoxy solutions: Scan rate is 10 °C/min.

by liquid−liquid phase separation,[5,18] as previously reported by Venderbosch.[5]

Thermal analysis also provides information on demixing and vitrification. After a quench, the PPE/epoxy blend behaves as a two-component system which gives two separate T_g's as shown in Figure 4. The mixture with 60 wt % PPE shows two transition temperatures at −5 and 110 °C, which are associated with the T_g of the PPE-rich phase and epoxy-rich phase. When thermal analysis is performed on a 20% solution of PPE, only the lower T_g is observed. The DSC results indicate that the vitrification of the PPE-rich phase occurs when the phase reaches the Berghmans point,[19] which is the intersection between the coexistence curve and T_g−composition line defined by the Fox equation,[20] and no further phase separation is possible. As expected, no thermal transition associated with phase separation was observed, and this is due to the nature of the small heat of mixing. Even in a monodisperse polymer blends, the exothermic peak of demixing is usually broadened.[21]

Figure 5 illustrates the predicted and experimental phase diagram and T_g−composition relation for the PPE/epoxy system. As often found for blends of polydisperse polymer, the cloud point curve is suppressed relative to the prediction from Flory−Huggins theory.[22] Moreover, due to the polydispersity of PPE and epoxy resin, the actual cloud point curve is broader than the calculated curve. A critical point of 8.3% PPE at 216 °C is obtained from the Flory−Huggins equation. The Flory−Huggins χ parameter can be calculated from the results of the onset of phase separation and the T_g−composition relationship, assuming its temperature dependence to be $\chi = A + B/T$. Figure 6 illustrates the χ parameter for PPE/epoxy mixture as a function of $1/T$ where T is the absolute temperature. The line is fitted to the following equation:

$$\chi = 145/T + 0.002 \qquad (1)$$

using values of the degree of polymerization of the PPE and epoxy resin as 242 and 2, respectively. The func-

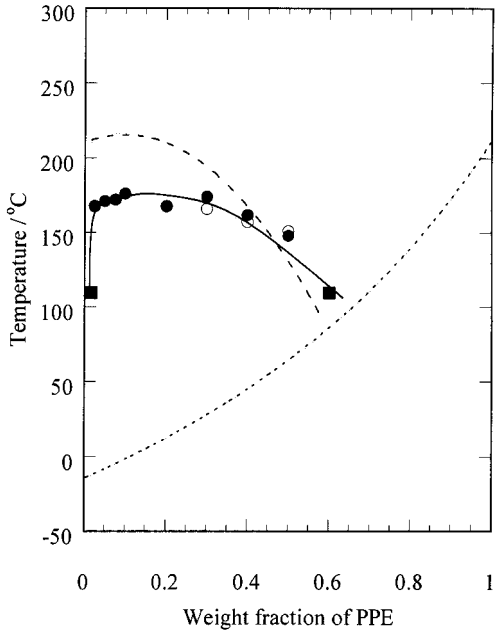

Figure 5. Phase diagram of the PPE/epoxy blend from optical microscopy (●), rheology (○), and DSC (■). The solid line is a guide to the eye through the experimental points. The dashed line is calculated via Flory−Huggins theory. The dotted line is the T_g−composition curve predicted according to the Fox equation.[21]

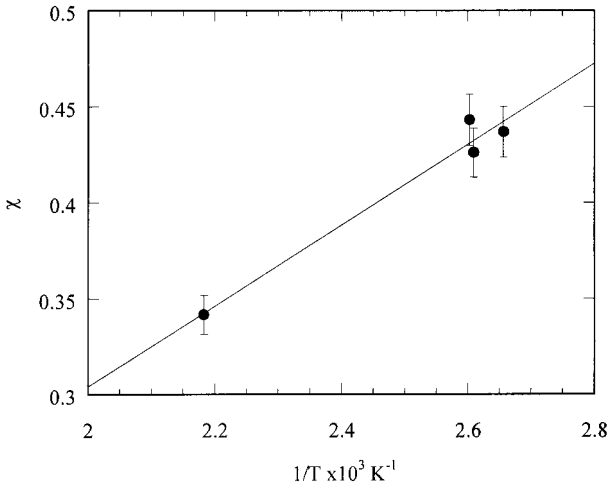

Figure 6. Temperature dependence of χ parameter for the PPE/epoxy mixture as estimated from onset of phase separation and the composition of phases from DSC.

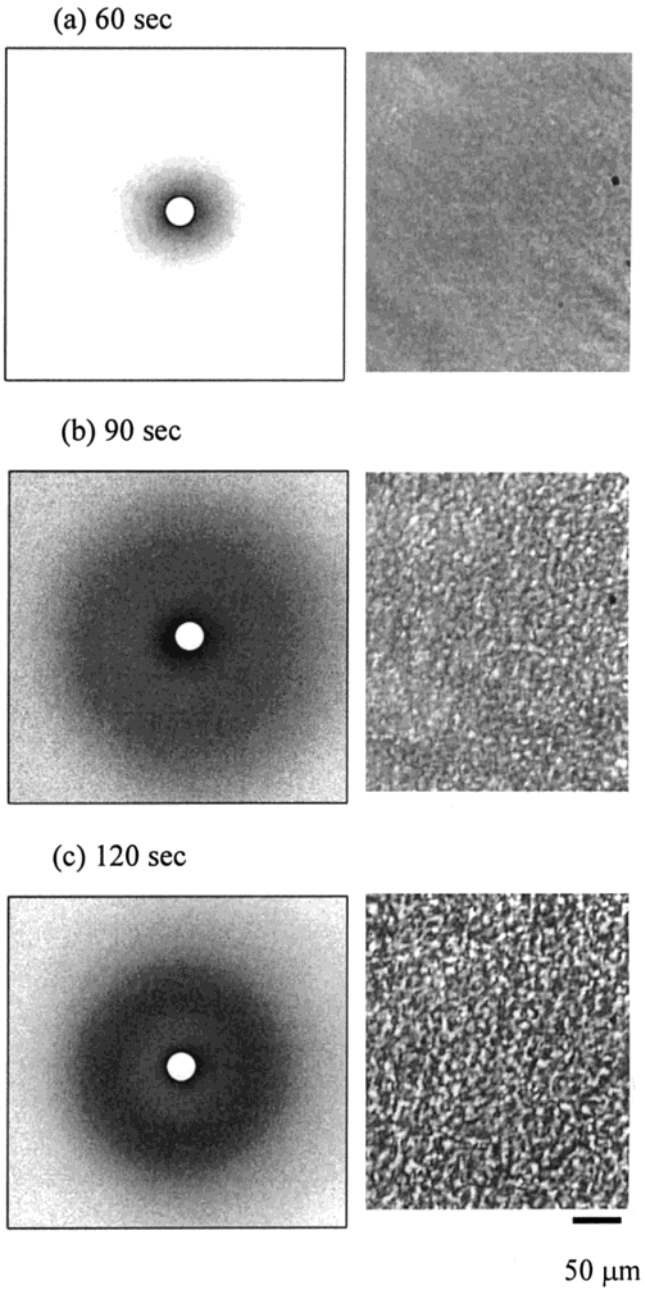

Figure 7. Light scattering patterns from the PPE/epoxy blend and corresponding optical micrographs during isothermal curing of a 30% PPE blend at 195 °C.

tional form of $\chi(T)$ is typical of that seen for UCST behavior, and the coefficients are reasonable compared to those reported previously for thermoplastics in epoxy resin.[8]

The Berghmans point is significant for considering phase diagrams of polymers because once the composition reaches this point, no further phase separation is possible. The experimental cloud point curve gives the Berghmans point, at 100 °C with a PPE/epoxy ratio of 0.63, which is in good agreement with that of the calculated point at 90 °C of 0.58. The phase diagram indicates that homogeneous solutions of PPE and epoxy resin can be obtained below 200 °C.

Time-Resolved Light Scattering. Figure 7 presents typical light scattering patterns from a 30 wt % PPE/epoxy blend and the corresponding optical micrographs during isothermal curing at 195 °C. Initially, the sample has no excess scattered intensity, and the corresponding optical micrograph shows homogeneity. After a certain time, the light scattering pattern starts to develop a characteristic azimuthally symmetric spinodal ring that increases in intensity and decreases in scattering angle with time. The corresponding real space images also show that phase separation is occurring during processing. The ring pattern and the characteristic change in scattering profiles are signatures of spinodal decomposition. Figure 8 shows azimuthally averaged variation of light scattering profiles with curing at 195 °C. An intensity maximum appears at the onset of phase separation, and the peak maximum moves to lower q with increasing time. Figure 9 shows the time course of the measured scattering invariant, $Q = \int I(q)q^2\,dq$, during isothermal curing. In the following sections, a four-stage model is discussed: (a) reaction prior to phase separation, (b) early stage spinodal

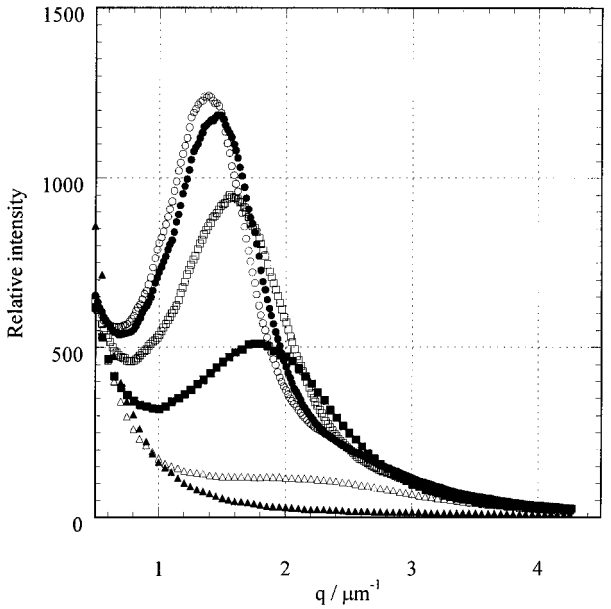

Figure 8. Scattering curves for a 30 wt % PPE blend after curing at 195 °C for 60 s (▲), 90 s (△), 120 s (9), 150 s (□), 180 s (●), and 210 s (○).

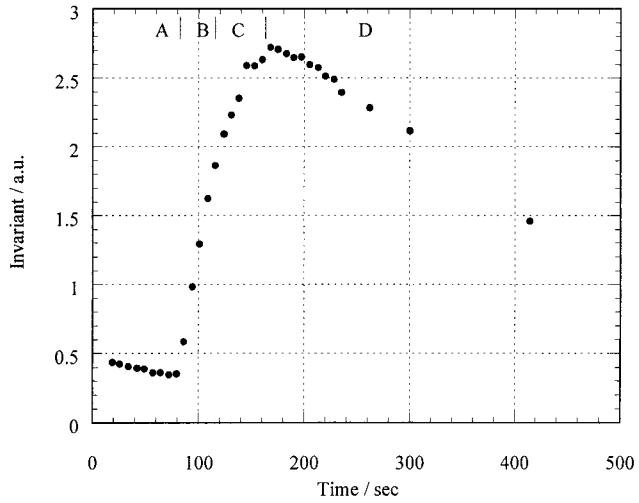

Figure 9. Scattering invariant as a function of time during isothermal curing of a 30% PPE blend at 195 °C. The four stages are shown on the top of the figure: (a) onset of phase separation, (b) early stage of spinodal decomposition, (c) late stage of spinodal decomposition, and (d) apparent phase dissolution.

decomposition, (c) late stage spinodal decomposition, and (d) refractive index changes and apparent phase dissolution.

(a) Reaction Prior to Phase Separation. The initial stages of the polymerization occur in a homogeneous phase, building epoxy molar mass. At some critical extent of reaction phase separation occurs, and the onset time and conversion of epoxy resin, which were measured by light scattering and in-situ DSC, respectively, are listed in Table 1. The extent of reaction at the onset of phase separation increases with the weight fraction of PPE and also the curing temperature. For thermally induced phase separation, spinodal decomposition requires an appropriate quench depth which is usually given by a thermal jump. However, reaction-induced phase separation takes place under progressive increases in quench depth. The extent of reaction at the onset of the phase separation is regarded as the minimum quench depth for spinodal decomposition. This means that the temperature dependency of the extent of reaction at constant composition can be regarded as a required chemical quench for spinodal decomposition.

Table 1. Characteristic Parameters for Reaction Induced Phase Separation in PPE Epoxy Blends[a]

T_{cure}	w_{PPE}	t_ϕ	p_ϕ	$10^3 D_{eff}$	$q_m(0)$	α
175	30	70 ± 5	1.5 ± 0.3	1.3 ± 0.1	2.5 ± 0.1	0.28 ± 0.01
175	40	114 ± 5	2.7 ± 0.2	0.9 ± 0.2	2.8 ± 0.2	0.39 ± 0.01
175	50	216 ± 5	5.3 ± 0.2	0.4 ± 0.1	2.6 ± 0.2	0.29 ± 0.02
195	30	79 ± 5	2.1 ± 0.4	2.1 ± 0.2	4.2 ± 0.2	0.25 ± 0.03
195	40	101 ± 5	4.8 ± 0.4	0.9 ± 0.1	3.2 ± 0.1	0.37 ± 0.02
195	50	158 ± 5	7.8 ± 0.4	0.3 ± 0.1	2.2 ± 0.2	0.18 ± 0.01

[a] Curing temperature, T_{cure} (°C); PPE content, w_{PPE} (%); phase separation time, t_ϕ (s); phase separation conversion, p_ϕ (%); effective diffusion coefficient, D_{eff} (μm s^{-1}) ; initial scattering peak position, $q_m(0)$ (μm^{-1}) ; late stage power-law exponent, α.

Figure 10a,b illustrates the phase diagrams and explains the chemical quench in this system. Because of the difference in the molecular weight between PPE and epoxy resin, the cloud point curve and spinodal line are asymmetric and located in the lower concentration region (on the left side of the phase diagram for PPE). In Figure 10a, once the reaction starts, the spinodal line moves upward due to the increase of molecular weight of epoxy resin. We have to move the spinodal line to the point *P* for spinodal decomposition to occur at that temperature and composition. The distance from the spinodal line to the point *P*, indicated as an arrow in Figure 10a, is regarded as a required chemical quench depth for spinodal decomposition. In Figure 10b, three different curing conditions are put on the phase diagram. The points *A* and *B* are the same curing temperature; however, the weight fractions of the PPE are *B* > *A*. The points *A* and *C* are the same composition; however, curing temperatures are *C* > *A*. In each case the quench depth is given by the arrow, in Figure 10b, which is the shortest connection between the point at fixed temperature and composition and the spinodal boundary at the beginning of the reaction. In the case of reaction-induced phase separation the quench depth required for spinodal decomposition maps onto the reaction conversion. Thus, the quench depths are *C* > *A* and *B* > *A*, and the conversion at the onset of phase separation is seen to increase (Table 1) with PPE content and curing temperature.

(b) Early Stage of Spinodal Decomposition. If, as discussed earlier, the phase diagram is assumed to be a pseudobinary, Cahn−Hilliard theory[13] can be applied to the early stage of spinodal decomposition as development of scattering intensity follows:

$$I(q,t) = I(q,0)\exp[2R(q)t] \qquad (2)$$

where q ($=4\pi n/\lambda \sin(\theta/2)$) is the scattering wave vector which depends on the average medium refractive index n, radiation wavelength λ, and scattered angle θ. $I(q,t)$ is the scattered intensity at the wave vector q and time t, and $R(q)$ is the amplification factor. A representative semilogarithmic plot of intensity ($q = 1.5\ \mu$m^{-1}) vs time is plotted as an inset to Figure 11 for isothermal temperatures of 195 °C. The initial plateau is during the induction time when the homogeneous system is developing molecular weight. A regime where ln $I(q,t)$ is linear with time follows, and this is used to calculate

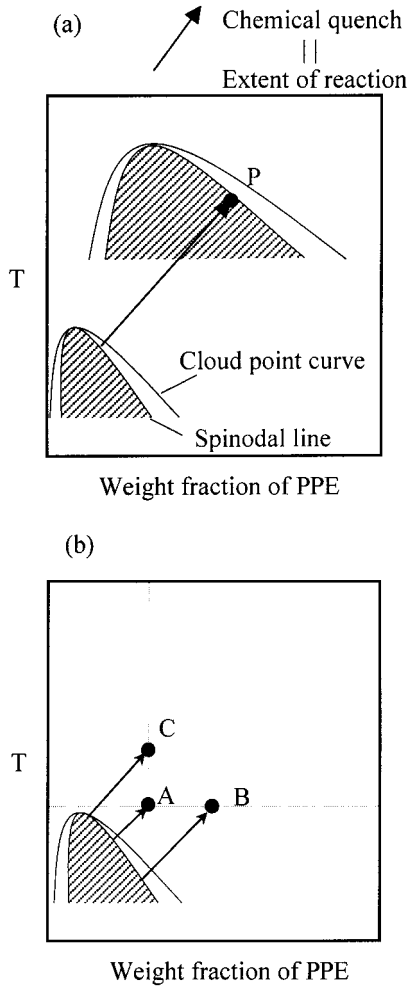

Figure 10. Schematic representation of the chemical quench depth. Because of the difference in the molecular weight between PPE and epoxy resin, the binodal and spinodal are asymmetric and located in the lower PPE concentration region. (a) As the reaction proceeds, the spinodal line moves to higher T and PPE concentration due to the increase of molecular weight of epoxy resin. The spinodal line must move past point P for spinodal decomposition to occur at that temperature and composition. (b) Three different curing conditions are shown, and the quench depth required for decomposition is given by the arrow, which is the shortest connection between the point at fixed temperature and composition and the spinodal boundary at the beginning of the reaction.

the amplification factor, $R(q)$. The growth of ln $I(q,t)$ with t becomes nonlinear in the late stage of spinodal decomposition. Okada and Han[23] reported that the linear theory is valid at the early stage for deeper quenching for thermally induced phase separation. The validity of the linear theory for this system is not obvious because the quench depth, defined by the extent of epoxy reaction, is continuously increasing. The growth in epoxy chain length has two opposite effects on phase separation kinetics: increasing quench depth speeds it up whereas increasing viscosity slows it down. The phenomenmology observed shows that systems with a shallow chemical quench have the characteristics of spinodal decomposition. Equation 2 relates the amplification factor $R(q)$ and scattering vector q. The set of amplification factors for various q are plotted as $R(q)/q^2$ vs q^2 in Figure 11 for a 30 wt % system at 195 °C. The data fit a straight line, suggesting the validity of the linear theory, and from such plots the initial correlation length and effective diffusion coefficients,

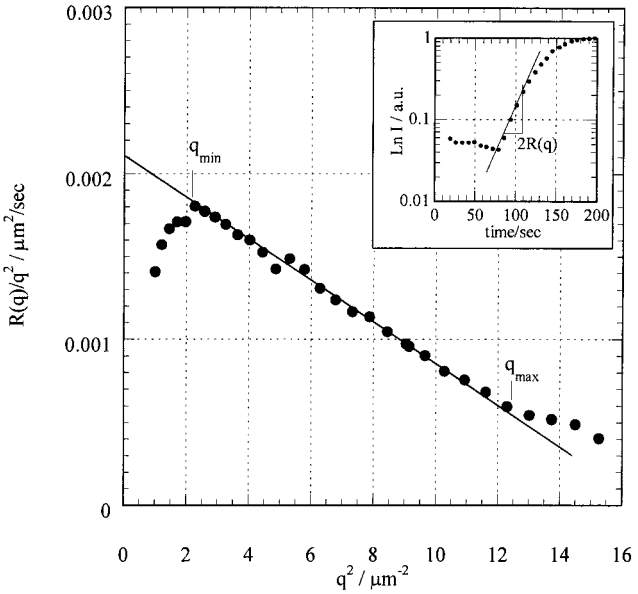

Figure 11. Analysis of the scattered intensity during the early stage of spinodal decomposition according to linearized Cahn−Hilliard theory. A plot of $R(q)/q^2$ versus q^2 is fitted to a straight line in the limits of q_{min} to q_{max}. The apparent diffusion coefficient is estimated from the $q = 0$ intercept. The inset shows how $R(q)$ is obtained from the intensity−time data for $q = 1.5\ \mu m^{-1}$.

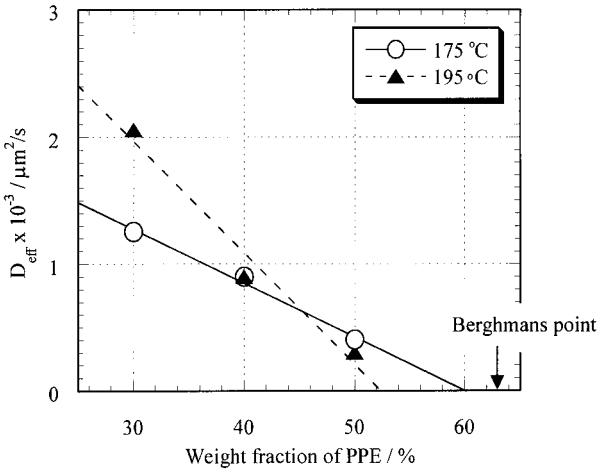

Figure 12. Concentration dependence of the effective diffusion coefficient derived from Cahn−Hilliard analysis of spinodal decomposition.

which characterize the early stage of spinodal decomposition, are obtained as listed in Table 1.

Figure 12 plots the effective diffusion coefficient versus weight fraction of PPE for 175 and 195 °C. The diffusion constant increases with the curing temperature and reduces to zero when the PPE content is 60 wt %; experimentally, the Berghmans point was found at 63 wt % PPE. The Berghmans point is at the intersection of the T_g−composition line and the cloud point curve and should have some temperature dependence, which is discussed in the following paper;[24] however, the point should reflect the vitrification of the PPE/epoxy mixture. This indicates that the kinetics of spinodal decomposition are influenced by the vitrification process of the system. One method to account for the influence of the relaxation dynamics of the system is to apply a WLF-type correction to the observed diffusion coefficient.[25] This is not appropriate in this

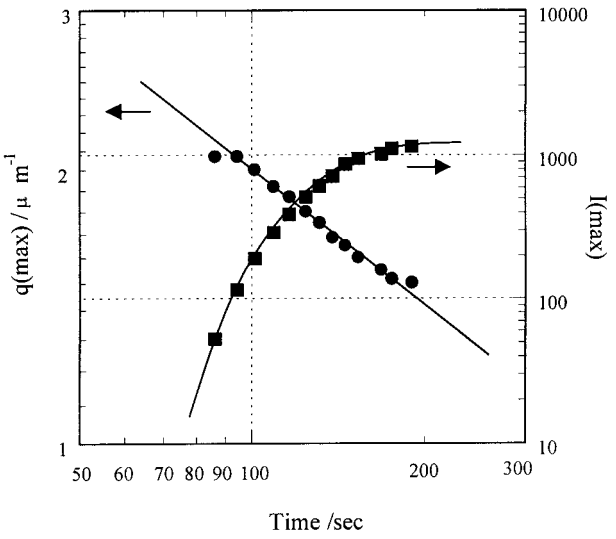

Figure 13. Variation of q_m and I_m with time in the late stage of spinodal decomposition during isothermal curing of a 30% PPE blend at 195 °C.

case due to the reacting nature of the polymer solution, which continuously changes T_g and thus the relaxation time.

(c) Late Stage of Spinodal Decomposition. The onset of the late stage is signaled by the failure of the linear approximation assumed in eq 2. During the late stage, the maximum of the scattering vector, q_m, starts to decrease with time: thus, the characteristic wavelength of the spatial composition fluctuations increases with time, and the maximum intensity, I_m, starts to deviate from the exponential increase with time in such a way that the rate of the intensity increase tends to slow down.[26]

In the late stage of the spinodal decomposition, several theoretical treatments have been applied. Langer[27] predicts that q_m should fit a power-law expression with t,

$$q_m \sim t^{-\alpha} \tag{3}$$

where $\alpha = 0.21$. Binder[28] predicts the power-law relationships of q_m and I_m on the basis of cluster dynamics,

$$q_m \sim t^{-\alpha} \, I_m \sim t^{-\beta} \tag{4}$$

such that $\alpha = {}^1/_3$ and $\beta = 1$.

Figure 13 represents the typical variation of q_m and I_m with time on curing. The maximum of the scattering

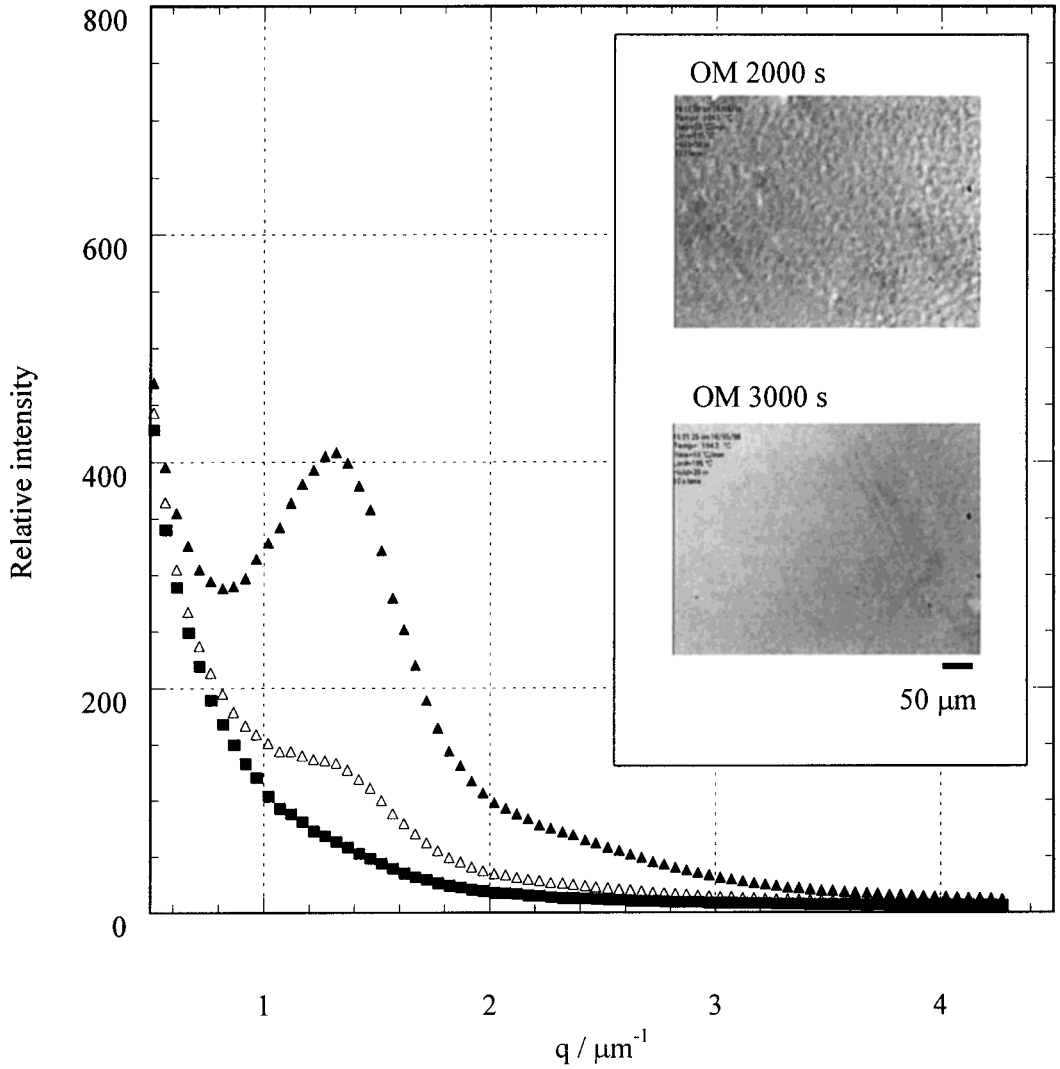

Figure 14. Scattered intensity profiles after 600 s (▲), 900 s (△), and 1200 s (■) during isothermal curing of a 30% PPE blend at 195 °C. The insets are optical micrographs at 2000 and 3000 s illustrating the loss of optical contrast.

vector fits the power-law expression over the full time range, but it should be noted that this is less than 1 decade in time and only a factor of 2 in peak position. The peak intensity is not a power law over any reasonable time interval, and this is due to the changes in refractive index, which is discussed in the following section. Table 1 lists the index of the power law on q_m. The results do not show unambiguous agreement with either theory; however, these data seem to fit a little better to Binder's cluster dynamics.

(d) Reactive Index Changes and Apparent Phase Dissolution. After the intensity of scattering light has reached a maximum, it starts to decrease with time. Figure 14 shows the change in the light scattering profile with time in the late stage. The peak intensity decreases without a substantial change in position, and finally the scattering peak disappears. This apparent phase dissolution is also confirmed by the optical micrographs shown in the inset to Figure 14. The apparent phase dissolution phenomena was first reported in PES/epoxy system by Inoue et al.[29] and is caused by a large change in the refractive index of the epoxy resin during cross-linking. The total scattered intensity, the invariant, Q, is given by the volume fractions and refractive indices of the phases.

$$Q = \int I(q)q^2 \, dq \propto \phi(1 - \phi)(\Delta n)^2 \qquad (5)$$

where $\Delta n = n_{PPE} - n_{epoxy}$ is a refractive index difference of the phases and ϕ is the volume fraction of PPE-rich phase. As the reaction proceeds, the epoxy becomes more dense and n_{epoxy} gets close to n_{PPE} and the total scattered intensity decreases. A zeroth-order model of the scattering would at least require the density and n_{epoxy} to be known as a function of conversion. While these are measurable quantities the measurement of phase compositions and volume fractions from scattering requires refractive index difference of the phases to be known, and this is not directly measurable. The change in Δn may affect the peak intensity in the late stage of spinodal decomposition and causes the discrepancy between I_m and the theoretical prediction in the late stage. The fact that the material still has a two-phase morphology is apparent in the SEM micrographs in Figure 15 which shows the cross-sectional view of the cured mixture before (a) and after rinsing with chloroform (b). Since PPE is completely soluble in chloroform, the image in Figure 15b supports hypothesis that the continuous phase is a PPE-rich phase, as reported previously.[5−7]

Secondary phase separation may take place in reaction-induced phase separation, and this results in dispersed phase particles with inclusions of the continuous phase material.[8] Clarke[30] and co-workers have simulated the phase behavior of linear/branched polymer blends and predict secondary phase separation. The secondary phase separation process occurs when the blend first passes into the metastable region and then into the unstable region such that some nucleation and growth precedes spinodal decomposition, or more interestingly, the composition of the coexisting phases changes due to continued cross-linking such that they themselves become unstable. Figure 16 shows a TEM micrograph at high magnification. Obviously, only the continuous PPE-rich phase and droplet epoxy-rich phase are observed, and no secondary phase separation was observed. From these results it is not unambiguously known whether secondary phase separation occurs in the PPE/epoxy blends, and both theoretical and experimental approaches should be followed in further work on this subject. The high degree of phase separation is confirmed by the dynamic mechanical properties of a cured blend containing 30 wt % of PPE shown in Figure 17. For the blend, two distinct loss peaks are observed at 130 and 190 °C, corresponding to the T_g's of the dispersed epoxy-rich phase and the PPE-rich matrix, respectively.

(a)

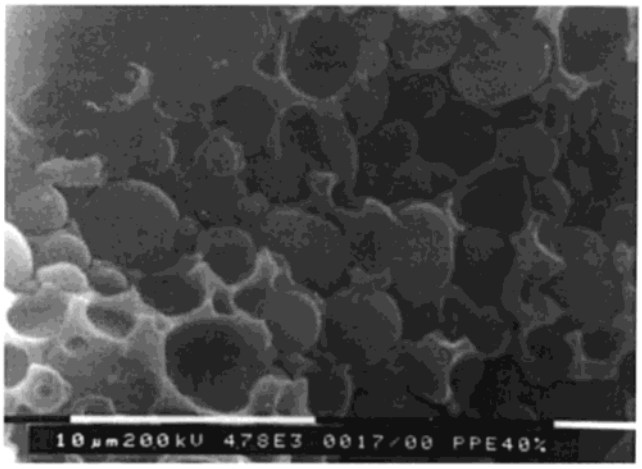

(b)

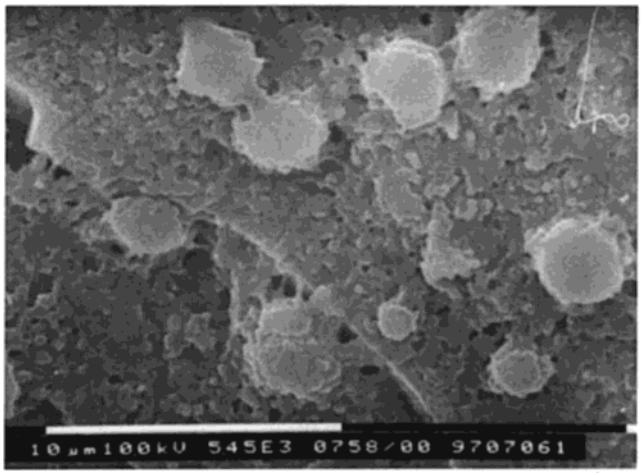

Figure 15. Scanning electron micrographs of fracture cross sections views of a 30% PPE blend showing the continuous phase is PPE-rich: (a) cured at 200 °C and (b) after rinsing with $CHCl_3$.

Conclusions

Reaction-induced phase separation of PPE/epoxy blends was investigated using a time-resolved, small-angle light-scattering camera equipped with a DSC sample holder. A four-stage model was discussed: (a) reaction prior to phase separation where the critical extent of reaction is the chemical quench for spinodal decomposition; (b) early stage spinodal decomposition where the scattering intensity increases exponentially with time and the Cahn−Hilliard linear theory can be applied to the system, (c) late stage spinodal decomposition where the peak position shows a power law with time, and (d) apparent phase dissolution where the scattering intensity starts to decrease with time caused by a large

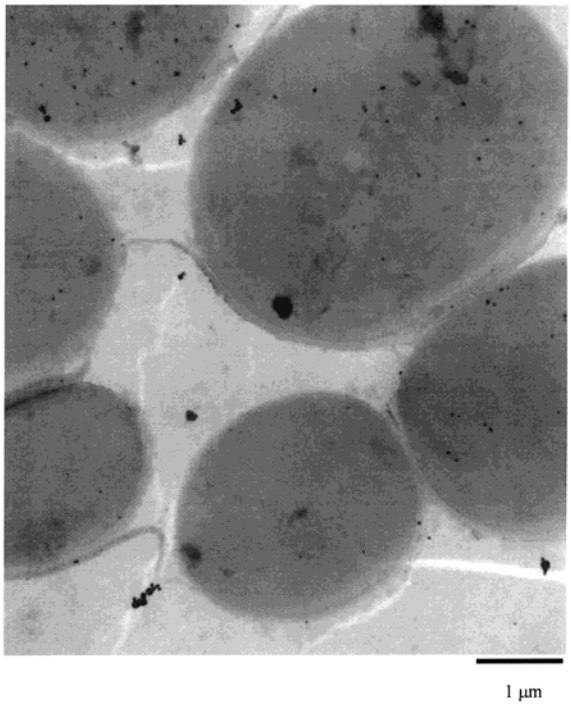

Figure 16. Transmission electron micrograph of a 30 wt % PPE blend cured at 200 °C.

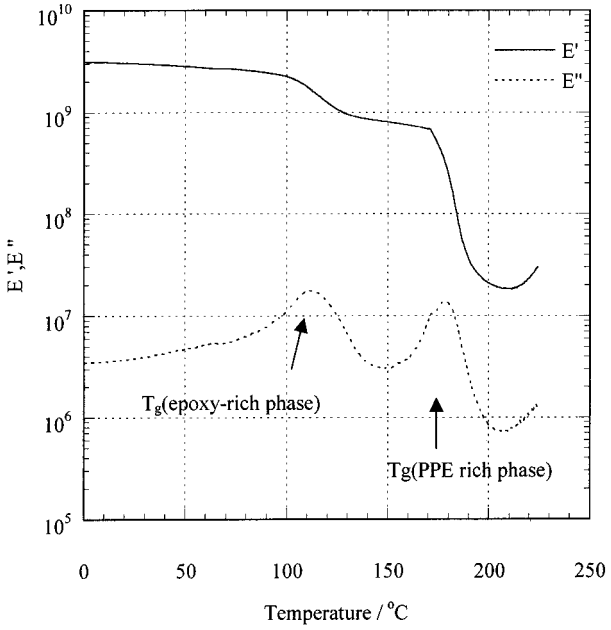

Figure 17. Plot of in-phase, *E′*, and out-of-phase, *E″*, modulus of a 30 wt % PPE blend cured at 195 °C.

change in the refractive index of the epoxy resin. The morphology of the cured blend was confirmed by SEM, TEM, and DMTA. The microscopy images and mechanical property measurements support the hypothesis that phase inversion occurred in reaction-induced phase separation, the PPE-rich phase is continuous, and the epoxy-rich phase is droplets. Our research is aimed at an understanding of both physical and chemical events during processing of PPE/epoxy blends in order to exercise control. The time-resolved, light scattering camera equipped with optical DSC is a powerful tool to investigate reaction-induced phase separation and can be applied for other thermoplastic/thermoset blends. The solidification mechanism of the PPE/epoxy blend is another aspect of the investigation, and this is reported in the following paper using chemorheological techniques.

Acknowledgment. This research was financially supported by Asahi Chemical (Japan) and the University of Sheffield. The authors thank R. W. Richards, R. A. L. Jones, and S. M. Clarke for their support in the design, and N. J. Terrill, C. Lumley, and R. Wilkinson for their help in construction, of the time-resolved light scattering instrument.

References and Notes

(1) Bowden, M. J., Turner, S. R., Eds. *Electronic and Photonic Application of Polymers*; American Chemical Society: Washington, DC, 1988.
(2) Reichmanis, E., Ed. *Microelectronics Technology, Polymer for Advanced Imaging and Packaging*; ACS Symposium Series 614; American Chemical Society: Washington, DC, 1995.
(3) Proceedings European PCB Convention, European Institute for Printed Circuit, 1998.
(4) *Encyclopedia of Polymer Science and Technology*, 2nd ed.; John-Wiley&Sons: New York, 1988; Vol. 13, p 1.
(5) Venderbosch, R. W.; Meijer, H. E. H.; Lemstra, P. J. *Polymer* **1994**, *35*, 4349.
(6) Venderbosch, R. W.; Meijer, H. E. H.; Lemstra, P. J. *Polymer* **1994**, *36*, 1167.
(7) Venderbosch, R. W.; Meijer, H. E. H.; Lemstra, P. J. *Polymer* **1994**, *36*, 2903.
(8) Williams, R. J. J.; Rozenberg, B. A.; Pascault, J.-P. *Adv. Polym. Sci.* **1997**, *128*, 95.
(9) Elwell, M. J.; Ryan, A. J.; Grünbauer, H. J. M.; Van Lieshout, H. C. *Macromolecules* **1996**, *29*, 2960.
(10) Lipatov, Y. S.; Grigor'yeva, O. P.; Konernik, G. P.; Shilov, V. V.; Sergeyeva, L. M. *Makromol. Chem.* **1985**, *186*, 1401.
(11) Yamanaka, K.; Takagi, Y.; Inoue, T. *Polymer* **1989**, *60*, 1839.
(12) Kim, B. S.; Chiba, T.; Inoue, T. *Polymer* **1993**, *34*, 2809.
(13) Cahn, J. W.; Hilliard, J. E. *J. Chem. Phys.* **1958**, *28*, 258.
(14) Griffith, I. W. Ph. D Thesis, UMIST, 1996.
(15) Ishii, Y. Ph. D Thesis, The University of Sheffield, 1999.
(16) Bras, W.; Derbyshire, G. E.; Devine, A.; Clark, S. M.; Cooke, J.; Komanschek, B. E.; Ryan, A. J. *J. Appl. Crystallogr.* **1995**, *28*, 26.
(17) URL: http://srs.dl.ac.uk/fcis/ccps.html.
(18) Bates, F. S. *Macromolecules* **1984**, *17*, 2607.
(19) Callister, S.; Keller, A.; Hikmet, R. M. *Makromol. Chem., Makromol. Symp.* **1990**, *39*, 19.
(20) Fox, T. G.; Loshaek, S. *J. Polym. Sci.* **1955**, *15*, 371.
(21) Vandweerdt, P.; Berghmans, H.; Tervoort, Y. *Macromolecules* **1991**, *24*, 3547.
(22) Oolabasi, O.; Robeson, L. M.; Shaw, M. T. *Polymer−Polymer Miscibility*; Academic Press: New York, 1979.
(23) Okada, M.; Han, C. C. *J. Chem. Phys.* **1986**, *85*, 5317.
(24) Ishii, Y.; Ryan, A. J. *Macromolecules* **2000**, *33*, 167.
(25) Bates, F. S.; Wiltzius, P. *J. Chem. Phys.* **1989**, *91*, 3258.
(26) Hashimoto, T.; Kumaki, J.; Kawai, H. *Macromolecules* **1983**, *16*, 641.
(27) Linger, J. S.; Bar-on, M.; Miller, H. D. *Phys. Rev. Lett.* **1987**, *59*, 668.
(28) Binder, K. *Phys. Rev. A* **1984**, *29*, 341.
(29) Kim, B. S.; Chiba, T.; Inoue, T. *Polymer* **1995**, *36*, 67.
(30) Clarke, N.; McLeish, T. C. B.; Jenkins, S. D. *Macromolecules* **1995**, *28*, 4650.

MA990837I